IL NUOVO CIMENTO Vol. 34 C, N. 1 Gennaio-Febbraio 2011
DOI 10.1393/ncc/i2011-10824-y

Colloquia: IFA 2010

Characterization of a radiographic system with broad energy band X-ray source

M. Gambaccini(1), P. Cardarelli(1)(*), G. Di Domenico(1), A. Taibi(1), M. Marziani(1), R. C. Barnà(2), L. Auditore(2), E. Morgana(2), D. Loria(2), A. Trifirò(2) and M. Trimarchi(2)

(1) *Dipartimento di Fisica, Università di Ferrara and INFN, Sezione di Ferrara via Saragat 1, I-44122, Ferrara, Italy*
(2) *Dipartimento di Fisica, Università di Messina and INFN, Gruppo Collegato di Messina I-98166, Messina, Italy*

(ricevuto il 9 Luglio 2010; approvato il 5 Agosto 2010; pubblicato online l'1 Marzo 2011)

Summary. — High energy X-ray beams with broad band energy spectra allow performing radiographic analysis on different materials and objects of relevant interest that cannot be investigated with conventional X-ray sources. The quality of a radiographic image strongly depends on the characteristics of the radiation source as the size of the X-ray emitting area, or focal spot, and the energy spectrum of the radiation. In this work the characterization of a broad-band energy bremsstrahlung source obtained from a linac providing a 5.5 MeV electron beam colliding with a tungsten target is presented. In order to measure the focal-spot size an *ad hoc* slit camera has been designed and built and a specific technique was used. Furthermore an analysis of the energy spectrum of the beam was performed using a method based on X-ray diffraction by a mosaic crystal.

PACS 07.85.Fv – X- and γ-ray sources, mirrors, gratings, and detectors.
PACS 52.59.Px – Hard X-ray sources.

1. – Introduction

The study of high-energy X-ray sources is a subject of primary interest in various fields of research. The opportunity of investigating heavy materials, aimed to make integrity analysis, non-destructive tests on industrial products, as well as studies on objects of relevant interest in cultural heritage, also demonstrated the need for a proper characterization of the X-ray beams. In this framework, the Istituto Nazionale di Fisica Nucleare (INFN) experiment DARMA is focused on material recognition, using a high-energy

(*) E-mail: cardarelli@fe.infn.it

bremsstrahlung photon beam produced by the 5.5 MeV electron linac operating at the Dipartimento di Fisica, Università di Messina [1].

The image quality of a high-energy radiography strongly depends on the beam quality (*i.e.* X-ray spectra) and focal-spot size, thus, the knowledge and proper setting of both parameters is crucial to reduce the uncertainties in the material recognition technique [2]. A rough experimental characterization of the linac X-ray beam quality is generally based on the Half Value Layer (HVL), obtained by measuring the attenuation curve of high-Z materials [3]. In fact spectroscopic measurements are very difficult to perform in a X-ray beam produced by an electron linac source for different reasons: photon flux, lack of proper detectors and proper collimation systems. Thus, a characterization of the beam energy distribution is generally made by Monte Carlo (MC) simulation [4, 5]. If a more accurate evaluation is needed a novel experimental method has to be investigated. One of this method has been tested using a technique based on the diffraction by a mosaic crystal. A description of this technique, the experimental setup and some preliminary results will be given in this work.

The focal spot, or the size of the target emitting X-rays, widely depends on the electron beam size and multi-scattering of electrons within the target. The use of the pin-hole or slit-camera technique is largely adopted in the field of diagnostic radiology, where low-energy X-rays are used [6, 7].

In order to use the slit-camera technique also for hard–X-ray beams a slit with adjustable width has been designed on purpose and used; experimental results will be discussed into this paper.

2. – Theoretical background

2˙1. *Measurement of the focal-spot size.* – The typical experimental setup used for measurement of the focal-spot size by means of the slit technique [8, 9] is reported in fig. 1. Consider I to be the total size of the focal-spot image, h the slit width and M the magnification ratio, then the focal-spot size f can be obtained as:

$$f = I/(M-1) - h(1-1/M). \tag{1}$$

This means that to obtain the size of the focal spot f, the knowledge of the slit width h is needed. When the energy of the X-ray beam is very high, it is not trivial to have negligible transmission of the slit edges, so the thickness of the absorbing material has to be large, the shape of the X-ray field transmitted by the slit is not sharp and the width h does not have a well-defined value.

If the slit aperture is narrow enough, *i.e.* $h \to 0$, the second term on the right hand of eq. (1) could be neglected, so the focal-spot size $f = I/(M-1)$.

This means that by measuring the image size I, or the FWHM of the X-ray intensity of the beam transmitted by the slit, by decreasing its width h, we could obtain the focal-spot size f, or its FWHM, by extrapolating to zero the slit width h.

2˙2. *Correction for the detector spread function.* – The radiation field $I(x, y)$ transmitted by the slit is converted to a radiographic image by the detector. The spatial distribution of the radiographic signal $R(x, y)$ is the convolution of the transmitted intensity $I(x, y)$ with the point spread function $\mathrm{PSF}(x, y)$ of the detector. The $\mathrm{PSF}(x, y)$ is the response of the detector to a point-like X-ray beam. The line spread function (LSF) is the response to a line input and it is defined as the integral of the PSF along the line

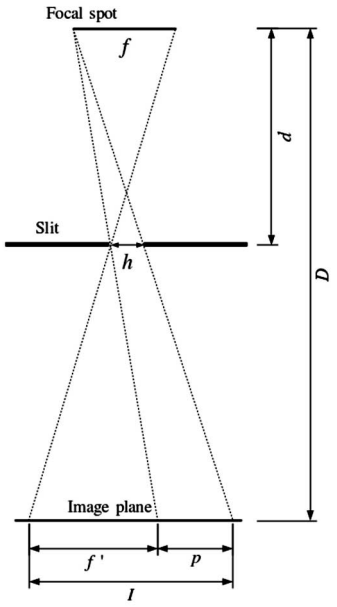

Fig. 1. – Typical geometrical setup for the focal-spot size measurement with the slit technique: focal-spot size (f), slit width (h), image size (I), penumbra (p) and focal-spot image (f').

direction. This means that along each direction of the slit image, the width of the slit profile will depend on the line spread function (LSF) of the X-ray detector. By supposing that both the profile and the LSF of the detector are Gaussian shaped we get

$$\mathrm{FWHM}_R{}^2 = \mathrm{FWHM}_I{}^2 + \mathrm{FWHM}_{\mathrm{LSF}}{}^2. \tag{2}$$

For very narrow slits ($h \to 0$) the hypothesis of Gaussian distribution of the profile is satisfied, so, by the knowledge of the $\mathrm{FWHM}_{\mathrm{LSF}}$ value, it is possible to obtain the width FWHM_I of the X-ray beam transmitted by the slit. To measure the LSF of the detector the edge response technique was used [10].

This technique permits to evaluate the LSF of the system using the edge spread function (ESF), obtained acquiring the image of an opaque object with a straight edge [11]. The measurement of the LSF is done by differentiating the analytical fit of the ESF, obtained from the image of a lead edge.

Assuming reasonably that the LSF is Gaussian shaped, it can be demonstrated that the LSF results in the form:

$$\frac{\partial(\mathrm{ESF})}{\partial x} = \mathrm{LSF}(x) = C \exp\left[\frac{(x - x_0)^2}{2\sigma^2}\right]. \tag{3}$$

For the purpose of this analysis we are just interested in the FWHM of the Gaussian LSF that is directly obtainable by the fit parameters of ESF. In fact performing a fit of the profile measured in the image with the function ESF, we directly obtain the FWHM of the Gaussian approximation of the LSF along that direction as $\mathrm{FWHM}_{\mathrm{LSF}} = 2.3548\ \sigma$.

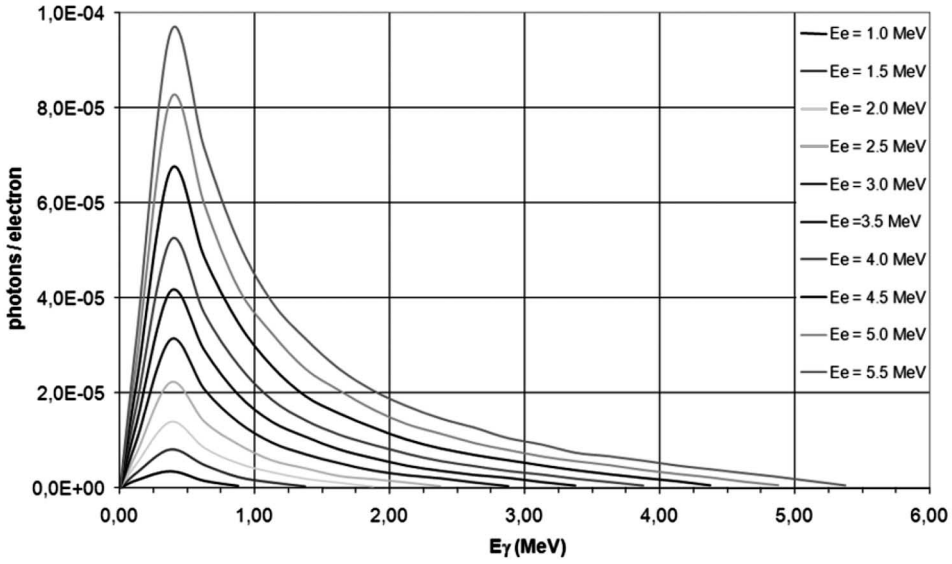

Fig. 2. – Bremsstrahlung spectra with different electron beam energy obtained with MC simulations.

2˙3. *Energy spectrum measurement.* – The image quality of high-energy radiography strongly depends on the beam quality (*i.e.* X-ray spectra), so it is important to characterize the energy distribution of the radiation produced. Both the spectrum and the angular distribution of the produced bremsstrahlung beam were simulated using a Monte Carlo code (MCNP, 4C2) [12]. In fig. 2 some of the X-ray spectra obtained with these simulations with various endpoint energy are shown [1]. Concerning the experimental test of these theoretical results, direct spectroscopic measurements in an X-ray beam produced by an electron linac source are very difficult to perform for different reasons: high photon flux, lack of proper detectors and proper collimation systems. The photon fluence expected at the detector distance, with an electron energy endpoint of 5 MeV, is about 10^3 photons $\cdot$ cm^{-2} per pulse, in pulses of 3 μs of duration. This leads to an instantaneous flux of about $3 \cdot 10^8$ photons $\cdot$ s^{-1} $\cdot$ cm^{-2}. A direct measure of a spectrum with such a high flux is clearly impossible with a common spectroscopic detector based on a scintillator crystal coupled to photo-multiplier or solid state devices. Common solutions for high-flux spectroscopy consist in increasing the distance between the detector and the source, or making use of collimation devices in order to reduce the irradiated area on the detector surface. However, in this case, increasing the distance in order to reduce the flux is not possible because of the laboratory size, and the realization of a highly collimated beam is complicated by the high energy of photons that requires a thick layer of absorber and produces a large amount of scattered radiation.

For these reasons it is not possible to make a direct measure of the energy distribution of the beam with a traditional spectroscopic detector, so a method based on the diffraction by a mosaic crystal has been developed.

2˙4. *Spectral analysis technique based on crystal diffraction.* – The basic idea is to extract a monochromatic beam from the primary beam using X-ray diffraction through

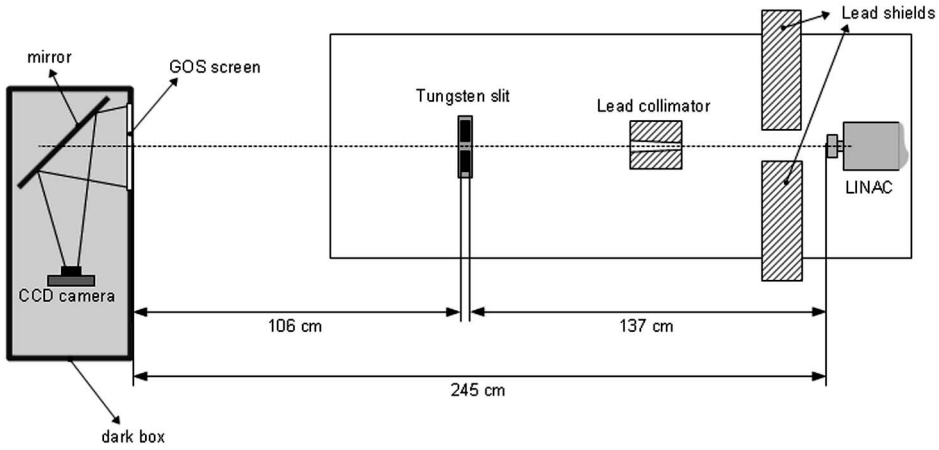

Fig. 3. – Layout of the experimental setup hosted at the Dipartimento di Fisica, Università di Messina.

a crystal. The energy of the diffracted beam depends on the positioning of the crystal, so by analyzing the intensity of the diffracted beam for different crystal positions it is possible to obtain information about the energy spectrum of the primary beam.

Let us consider Bragg's law for X-ray diffraction through a crystal:

$$2d \sin \theta_B = n\lambda, \tag{4}$$

where d is the lattice planes spacing, θ_B is the angle between the incident photon direction and the normal to the lattice plane, n is a integer positive number, λ is the wavelength of the incident radiation.

If then we consider a parallel X-ray beam with an arbitrary energy distribution impinging on a crystal oriented with an angle θ_B to the direction of the beam propagation, this will result in a diffracted beam made up of the photons having an energy that satisfies Bragg's law and that propagate with a angle $2\theta_B$ to the direction of the primary beam.

In this way it is possible to extract a monochromatic beam (except for the harmonics) with mean energy dependent only on the crystal lattice plane distance and Bragg's angle θ_B. The number of photons in the secondary beam is proportional to the number of photons of the primary beam in that energy band. Using the crystal characteristic rocking curve and the diffraction efficiency it would be possible to obtain quantitative information on the primary spectrum by measuring the intensities of the diffracted beam at different angles, *i.e.* different energies.

3. – Material and methods

3˙1. *Experimental setup for the focal-spot measurement.* – The experimental setup used for the focal-spot measurement is shown in fig. 3. X-rays are produced by a 5.5 MeV electron linac with a target made up of 1 mm of tungsten and 9 mm of copper. This system was optimized in order to provide the highest energy in photon production and to assure

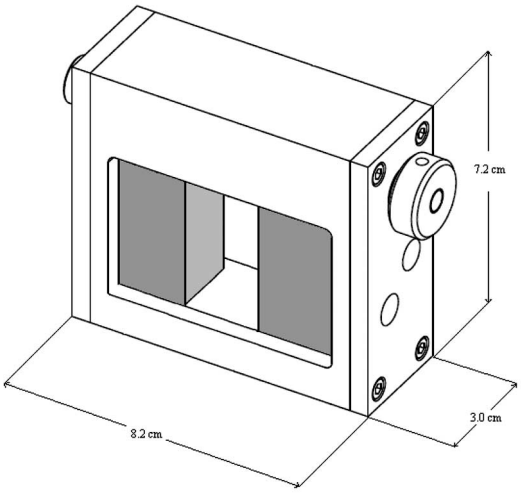

Fig. 4. – Slit with variable width, with two 20 mm thick tungsten edges.

proper heat dissipation. The collimated X-ray beam provides a circular irradiated field of about 16 cm diameter at the detector position [13].

The X-ray imaging system consists of a Gd_2O_2S:Tb (named GOS) fluorescent screen coupled to a high-resolution low-noise CCD camera (Alta Apogee E1). The CCD camera detects fluorescence light emitted by the GOS screen by means of an aluminum mirror tilted by a 45 degrees angle with respect to the beam direction. The size of a pixel on acquired digital images corresponds to $0.29 \times 0.29\,\mathrm{mm}^2$.

A layout of the slit is shown in fig. 4. It consists in an aluminum framework and two 20 mm thick tungsten edges. The slit width is continuously variable in the range 0–10 mm, and the tungsten thickness provides an attenuation of the X-ray beam of about one order of magnitude.

3˙2. *Experimental setup for the diffracted-beam measurement.* – The experimental setup for the diffraction measurement was similar to the one showed in fig. 3, with the only addition of the crystal mounted on a proper support placed after the tungsten slit, see fig. 5. The crystal used was a Cu (FCC) mosaic crystal with a mosaic spread of 0.005 degrees and 2.4 mm thick. The lattice plane used for diffraction was $(1, 1, 1)$ and the crystal was placed in Laue configuration, *i.e.* in transmission, as schematically depicted in fig. 5. The crystal support was equipped with three remote-controlled rotators in order to permit the correct orientation and alignment to the primary radiation beam. During the diffraction measurement, the slit aperture was set equal to 2.0 mm so the beam impinging on the crystal can be considered parallel with good approximation. The images of the diffracted beam were recorded with the imaging system previously described (subsect. **3**˙1).

4. – Results and discussion

4˙1. *Measurement of focal spot.* – Since the slit camera is far from the ideal model (negligible X-ray transmission and very narrow aperture), a whole set of image profiles

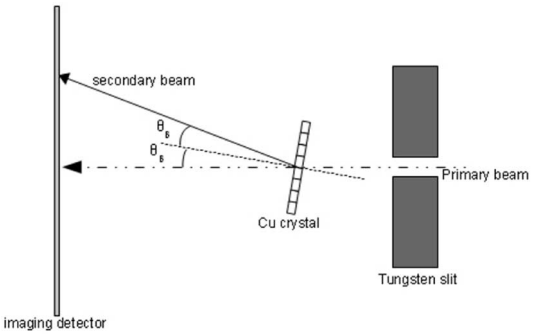

Fig. 5. – Experimental setup for the X-ray diffraction by a mosaic crystal (not to scale).

at different aperture width has been acquired and analysed. The adopted strategy is to consider each image profile and to calculate its FWHM as effective size of the focal-spot image I.

The images were acquired with standard HV settings for the electron linac (energy set to 5.5 MeV), nominal current of 30 mA, pulse length of $3 \cdot 10^{-6}$ s, and pulse rate of 1.5 Hz. The exposure time was set to 10 s per each slit aperture, and each image analysed is the average of 5 acquired images. The normalized profiles, obtained for slit aperture ranging from 1.50 mm to 0.15 mm, are reported in fig. 6. Through this procedure it is possible to obtain true image profiles and therefore a more realistic model that follows the expected theoretical trend of the image profile.

In order to complete the data analysis, a Gaussian fit of each image profile was calculated for slit width ranging from 0.30 mm to 2.50 mm. The zero intercept of linear

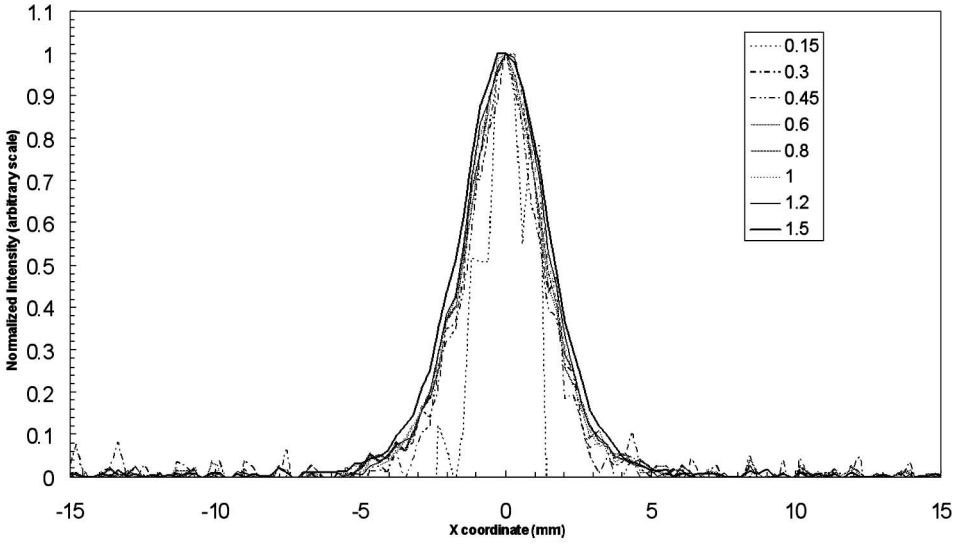

Fig. 6. – Plot of normalized image profiles obtained with a slit width ranging from 1.50 mm to 0.15 mm.

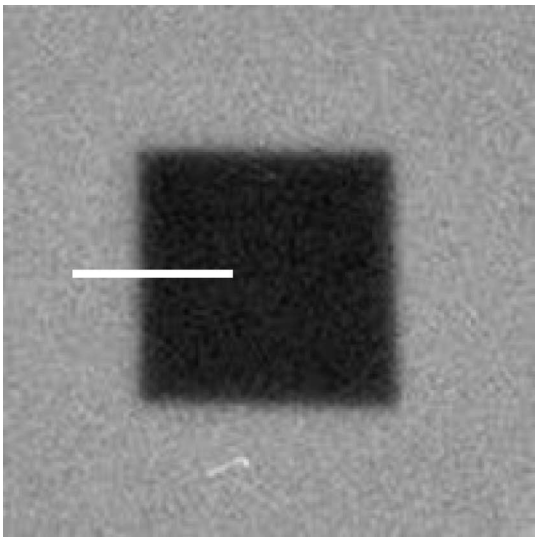

Fig. 7. – Image acquired with the lead test object, in *white* a sample of the profile used in this analysis.

regression of the FWHM data set gives the focal-spot size (FWHM) image of (2.78 ± 0.15) mm. The experimental uncertainties are mainly due to the procedures of correction and equalization of the acquired images [14].

4˙2. *Evaluation of the Line Spread Function.* – As previously described, in order to take into account the spread of the imaging system, a measurement of the LSF of the detector has been done measuring its edge response function. In this case the opaque object used was a lead square plate 2 mm thick placed in contact with the GOS screen (fig. 7). In the acquired image the areas containing the edge transition were isolated. In these areas the profiles obtained in single rows of pixels perpendicular to the edge were extracted, therefore these profiles were fit using eq. (3) as previously discussed in subsect. **2˙2** (fig. 8). This procedure was repeated for 50 pixel horizontal rows profiles centred at the edge transition in order to reach a satisfactory statistic sample. The result obtained for the FWHM of LSF was (1.63 ± 0.03) mm. Thus subtracting the LSF contribution to the extrapolated value obtained in subsect. **4˙1** using eq. (2) and then considering a magnification factor $M = 1.76 \pm 0.02$, using eq. (1), the resulting FWHM of the emitting area is (3.0 ± 0.4) mm.

4˙3. *Preliminary results of the spectrum measurement.* – The crystal and goniometers were aligned with the primary beam and various images at different angles θ_B were acquired with standard HV settings for the electron linac (energy set to 5.5 MeV); a nominal current of 30 mA, a pulse length of $3 \cdot 10^{-6}$ s, and a pulse rate of 1.5 Hz. The exposure time was set to 100 s for each position of the crystal.

In order to subtract the contribution of the primary beam in the image, we averaged a set of images with crystal placed at θ_B equal to zero and the result of this operation was subtracted to all the other images. After this operation the only visible contribution is given by the diffracted beam, as shown in fig. 9. In fig. 9 it is possible to see the diffracted beam (a) due to the vertical lattice plane $(1, 1, 1)$ and another diffracted beam (b) that

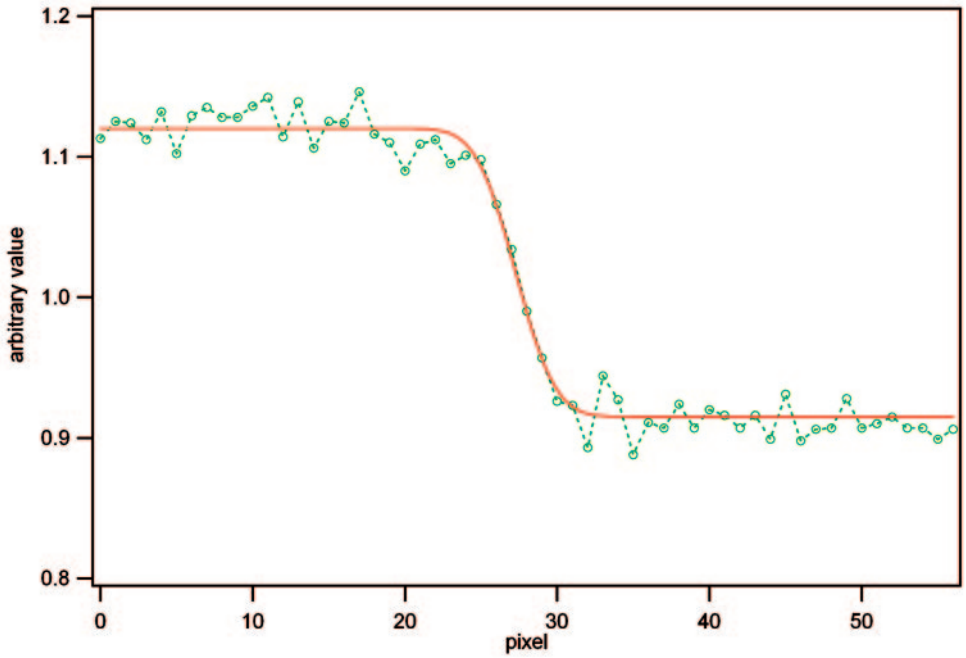

Fig. 8. – Result of ESF fit for a pixel row, fit function represented by the continuous line and dashed line and the markers represent the image profile.

was not considered in this analysis. By simple geometric considerations, by evaluating the distance from the centre of the primary beam, it is possible to set on the image an energy scale for the secondary beam.

The point of these results is to show that it is possible to extract a monochromatic beam with tunable energy by varying crystal angle θ_B, and to record an image of it. In order to perform a correct quantitative spectroscopic analysis with this technique, additional steps would be required:

- The rocking curve and absorption characteristics of the Cu mosaic crystal must be precisely known, in order to evaluate the number of primary photons from the fraction measured in the secondary beam in each energy band.
- Whether an imaging system is used to detect and record the diffracted beam, the relation between the energy fluence impinging on the imaging system and the grey level obtained must be evaluated using MC simulations, so as to use the grey level as a measure of photon fluence.
- The superior harmonics contribution must be evaluated, this could be done by acquiring a set of images of the diffracted beam with different filtrations and by analyzing the intensity results.

5. – Conclusions

We measured the focal-spot size of a linear accelerator by adapting the techniques commonly used in diagnostic radiology. An extrapolation method was successfully

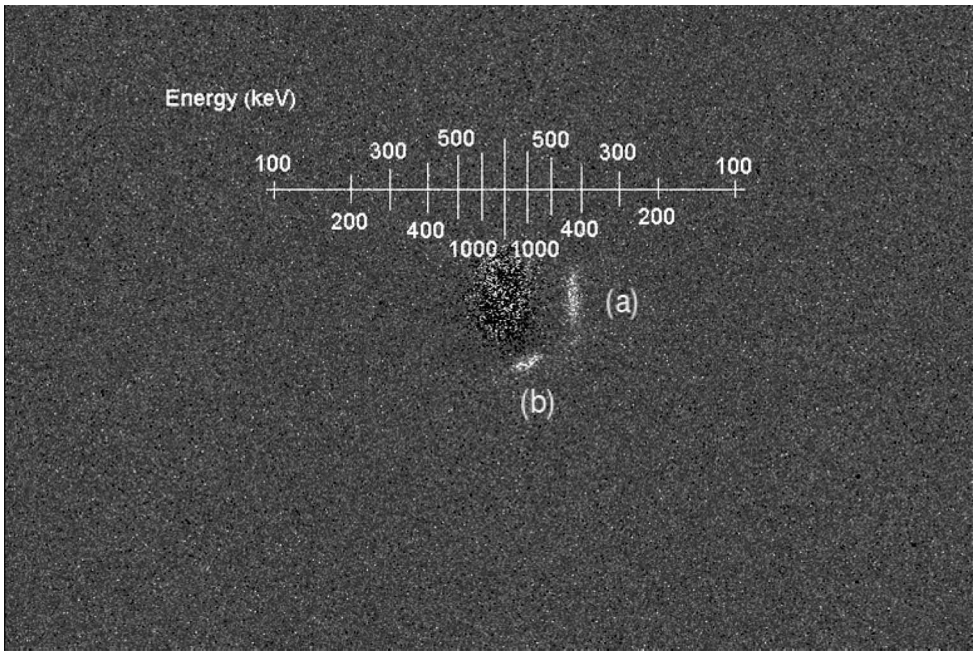

Fig. 9. – Image of the diffracted beam.

applied to account for the X-ray transmission of the slit walls. Furthermore, to avoid an overestimation of the focal-spot size, the spatial resolution properties of the X-ray imaging system were also measured.

We have also presented some preliminary results of a method to evaluate the energy spectrum in case of high flux that makes impossible using traditional spectroscopic techniques. As a first result this technique, based on X-ray diffraction through a mosaic crystal and an imaging system, showed that it is possible to extract a monochromatic diffracted beam that gives qualitative information about the energy spectrum, but with a further development of the theoretical model and further experimental tests it would be possible to obtain also quantitative information about the energy distribution.

REFERENCES

[1] Auditore L., Barnà R. C., De Pasquale D., Italiano A., Trifirò A. and Trimarchi M., *Phys. Rev. ST Accel. Beams*, **7** (2004) 030101.
[2] Miller jr. A. C., Cochran J. L. and Lamberti V. E., BWXTY-12, Y/DV1897 (2003).
[3] Jones H. E. and Cunningham J. R., *The Physics of Radiology*, fourth edition (Charles C Thomas Publisher, Springfield, Illinois, USA) 1983.
[4] Marziani M., Taibi A., Di Domenico G. and Gambaccini M., *Med. Phys.*, **36** (2009) 4683.
[5] Jabbari K., Sarfehnia A., Podgorsak E. B. and Seuntjens J. P., *Phys. Med. Biol.*, **52** (2007) 1171.
[6] Everson J. D. and Gray J. E., *Radiology*, **165** (1987) 261.
[7] Wagner R. F. *et al.*, *Phys. Med. Biol.*, **19** (1974) 241.

[8] Vaidya P. R., Mittal K. C. and Paithankar A. S., *Nucl. Instrum. Methods B*, **183** (2001) 497.
[9] Baird L. C., *Med. Phys.*, **7** (1980) 64.
[10] Boone J. M. and Seibert J. A., *Med. Phys.*, **21** (1994) 1541.
[11] Samei E. and Flynn M. J., *Med. Phys.*, **25** (1998) 102.
[12] *Monte-Carlo-N-Particle, version 4C2, code*, Diagnostics Applications Group, Los Alamos National Laboratory (Los Alamos, New Mexico, USA) and Radiation Safety Information Computational Center Oak Ridge National Laboratory (Oak Ridge, Tennessee, USA).
[13] Auditore L., Barnà R. C., De Pasquale D., Italiano A., Trifirò A. and Trimarchi M., *Nucl. Instrum. Methods B*, **240** (2005) 913.
[14] Tang S., Barnes G. T. and Tanner R. L., *Med. Phys.*, **22** (1995) 1803.